RSC Advances

ROYAL SOCIETY OF CHEMISTRY

www.rsc.org/advances

RSC Advances

ARTICLE

Fabrication of Stretchable, Flexible Conductive Thermoplastic Polyurethane/Graphene Composites via Foaming

Received 00th January 20xx,
Accepted 00th January 20xx

DOI: 10.1039/x0xx00000x

www.rsc.org/

Yuejuan Chen,[1] Yang Li,[1] Donghua Xu,[2*] Wentao Zhai[1*]

Stretchable and flexible conductive polymers have aroused great interest recently because their applications in the fields of novel electronics, such as smart textiles, artificial electronic-skin and flexible electronic displays, etc. In this work, stretchable and flexible conductive thermoplastic polyurethane (TPU)/graphene composite foams have been developed by water vapour induced phase separation. The as-prepared TPU/graphene composite foams exhibited lower modulus, larger elongation at break, and lower hysteresis during cycle tensile test than TPU/graphene composite did. It is expected that the improved elasticity of TPU/graphene composite foams was caused by the deformation of cells, which offset partially the deformation of TPU matrix. In addition, the cell walls divided the whole composites into many small parts, which could further restrain plastic deformation of hard segment domains under deformation.

1 Introduction

Recently, a class of stretchable electronic materials has aroused extensive interest because of their various applications in hi-tech fields of novel electronics, such as flexible strain sensors for human-motion detection and tactile sensors for electronic skins.[1,2] With stretchable smart sensors, sensitivity is the prerequisite and very precious. In addition, low hysteresis, high repeatability and excellent durability are still crucial to extend their lifetime.[3-5] Moreover, the sensors should be lightweight, and high stretchable to follow all the mechanical deformations of the textile materials without affecting the original textile characteristics such as softness, feel, etc. Among all the materials in research, conductive elastic composites (CECs) are one sort of materials respond to these specifications because of the advantages of stretch, mechanical robustness, lightweight and low-cost fabrication.[6,7] There are varieties of approaches to develop CECs, blending conductive fillers with elastic polymers is one of the most attractive methods due to the advantage of process simplicity, cost-effectiveness and tuning of conductivity. However, it is hard to simultaneously acquire high conductivity by increasing the proportion of conductive fillers and keep the outstanding mechanical and elasticity properties originated from elastic polymer,[8,9] which will eventually affect the repeatability and durability or sensitivity of the stretchable smart sensors. Other methods like filling micro-channels with liquid metals and infiltrating elastomers in conductive-filler networks,[10-14] may solve the problem, but will bring other problems like high cost or poor long time stability. Therefore, better solutions are needed to meet the requirement of smart sensors in human-motion detection.

Thermoplastic polyurethane (TPU) elastomers are multi-block copolymers composed of soft and hard segments, which are thermodynamic incompatibility at room temperature, and consequently, result in microphase separation. The elasticity of TPU, which can be characterized either by stiffness and strain recovery or hysteresis and stress relaxation inversely, is a crucial property in commercial competition with other thermoplastic elastomers.[15] In order to obtain more functionality, such as conductivity, high mechanical strength, many researchers prepared TPU based composites by adding functional nanofillers into the TPU matrix.[16-19] However, it is hard to find a win-win solution between acquiring high conductivity or high mechanical strength and achieving high strain at break. For example, Choi et al. found that the addition of functionalized graphene endowed TPU with high conductivity and the enhanced modulus, but reduced its tensile strength and elongation at break dramtically.[20]

Foaming is usually considered as an effect way to prepare lightweight materials and reduce the cost. There are many methods to introduce cell structure to TPU, such as in situ polymerization using water as foaming agent, batch foaming by CO_2, salt leaching, and phase inversion.[21-29] Among all of these, water vapour induced phase separation (WVIPS) is a facile and low-energy-consuming approach to prepare microcellular nanocomposites with both fine cell structure and high content of nanofillers.

Graphene, a newly discovered 2D carbon nanomaterial, not only possesses high Young's modulus but also exhibits high specific area and excellent electronic conductivity. These properties make graphene very promising in fabricating CECs,

[1]Ningbo Key Lab of Polymer Materials, Ningbo Institute of Material Technology and Engineering, Chinese Academy of Sciences, Ningbo, Zhejiang Province, 315201, China. E-mail: wtzhai@nimte.ac.cn
[2]State Key Lab of Polymer Physics and Chemistry, Changchun Institute of Applied Chemistry, Chinese Academy of Sciences, Changchun 130022, China. E-mail: dhxu@ciac.ac.cn

supercapacitors, thermoelectric materials, et al.[30-33] In this article, to prepare a stretchable conductive material, graphene was used to endow TPU with high strength and good electric conductivity. At the same time, microcellular structure was introduced to the TPU matrix by WVIPS method to obtain a better elasticity.

2 Experimental

2.1 Materials

TPU (E180) was purchased from Miracll Chemicals Co. (China), and dehydrated at 80 ℃ for 4 h. Graphene sheets with specific surface area of 700 m^2/g were prepared by the Staudenmaier's method as reported in our previous work.[34] Each graphene platelet was composed of 3–4 individual graphene sheets because the specific surface area is about 3.5 times lower than the ideal specific surface area (2630 m^2/g) of a single graphene sheet.[35] *N,N'*-dimethylformamide (DMF) was supplied by Sinopharm Chemical Reagent (China) and used as received.

2.2 Fabrication of TPU/graphene nanocomposites

A typical solution blending method was used to prepare the TPU/graphene nanocomposites (Fig. 1). First, a certain amount of graphene was dispersed in DMF with the assistance of ultrasonication for 90 min. Second, TPU pellets were added and stirred overnight at 70 °C. The resultant solution was added dropwise into excessive deionized water to get a precipitate of TPU/graphene nanocomposites. After filtrated and washed several times with deionized water, the precipitate was dried at 80 °C for 48 h to remove the residual water. Finally, the dried precipitate was disintegrated into powder for further experiment.

TPU/graphene nanocomposites (TPUG) were prepared by hot press at 200 °C, and then cooled in air. TPUG with 0, 5, 10, 15 and 20 phr (parts per hundred of resins) graphene were coded as TPUG0, TPUG5, TPUG10, TPUG15 and TPUG20, respectively.

2.3 Preparation of TPU/graphene nanocomposite foams

TPU/graphene composite foams were prepared by WVIPS as described in our previous work.[29] The as-prepared TPU/graphene powder with different concentration of graphene was dissolved in DMF under mechanical agitation for 24 h at 70 °C to form homogeneous solutions. After kept stilling for 30 min, the solution was cast into film on a flat glass and exposed in the air under a temperature of 20 °C and humidity of 80%. Then the solidified TPU/graphene foam sheets were immersed in cold water to remove the residual DMF and dried at 80 °C for 24 h. A series of TPU/graphene foams (TPUGF) containing 0, 5, 10, 15 and 20 phr graphene were prepared, and were coded as TPUGF0, TPUGF5, TPUGF10, TPUGF15 and TPUGF20, respectively.

2.4 Characterizations

The densities of TPUG and TPUGF were measured by the water displacement method according to ASTM D792. The hardness of all samples was measured by Shore A durometer according to ASTM D2240.

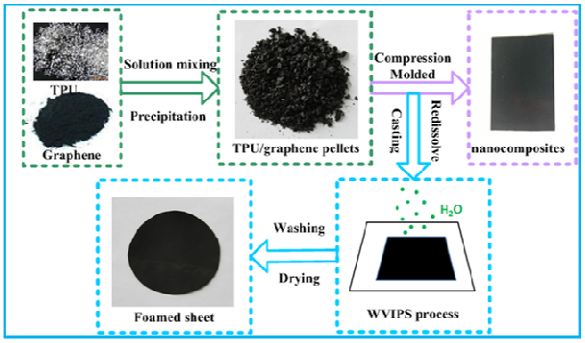

Fig. 1 Diagram for the preparation of the TPUG and TPUGF.

The foam morphology was observed by a Hitachi TM-1000 scanning electron microscope (SEM). The cell structure before and after cycle test was studied by a Hitachi S-4800 field emission SEM at an accelerating voltage of 4 kV.

The volume electrical conductivity of moderately conductive samples (> 1×10^{-8} S/cm) was measured using a standard four-probe method on a Napson Cresbox Measurement System. The samples with rather low conductivity (≤1×10^{-8} S/cm) were measured with three-terminal fixture on an EST121 ultrahigh resistance and microcurrent meter (Beijing EST Science & Technology CO. Ltd.) in accord with ASTM D257.

The mechanical and elasticity properties of the TPUG and TPUGF samples were measured using a universal testing machine Instron 5567, while all specimens were 100 mm × 10 mm × 1 mm and at least three specimens were tested for each sample. The elasticity is characterized by the hysteresis of the load-unload curves and residual strain in the cycle tensile test. To compare the hysteresis of different samples, cycle test at 25 mm/min was performed and the relative hysteresis of each sample was calculated. The relative hysteresis for a given cycle is calculated by the ratio of the area bounded by the loading-unloading curves to the total area under the loading curve.[36]

3 Results

3.1 Foam structure characterizations of TPUG and TPUGF

Table 1 shows the densities and hardness of TPUG and TPUGF. The density of TPUG slightly increases from 1.18 to 1.27 g/cm^3 with graphene loading increasing from 0 to 20 phr. After the foaming, however, the density of TPUGF is in the range of 0.39-0.41 g/cm^3, showing about three times volume expansion. The hardness of TPUG0 is about 78. After the addition of graphene, the hardness of TPUG significantly increases to a value exceeding 90. With the introduction of cell structure, however, the hardness of TPUGF reduces to a range of 36 to 55. It is obvious that foaming is an effective way to prepare lighter and softer TPU composites.

As indicated in Fig. 2a, the foamed TPUG sheets show good flexibility and can be folded and flattened easily under a weak force. Fig. 2b shows the fractured SEM images of TPUGF. It is

Table 1 Density and hardness of TPUG and TPUGF samples

Graphene content		Density (g/cm^3)		Hardness (shore A)	
(phr)	(wt%)	TPUG	TPUGF	TPUG	TPUGF
0	0	1.18	0.40	78	36
5	4.8	1.24	0.40	>90	44
10	9.1	1.25	0.41	>90	50
15	13.0	1.25	0.39	>90	52
20	16.7	1.27	0.40	>90	55

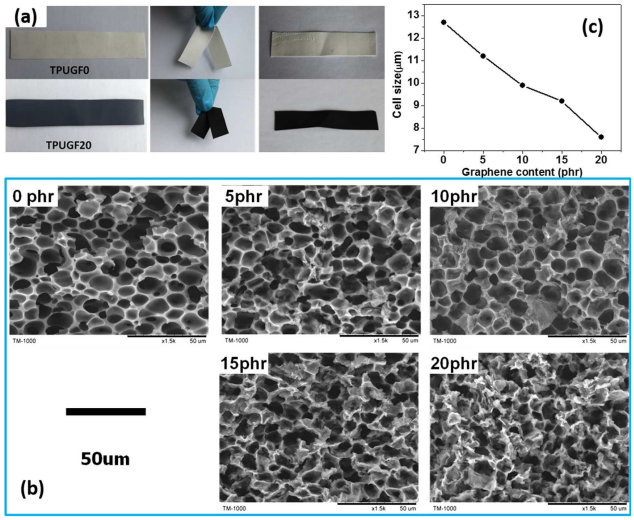

Fig. 2 Optical photographs (a), SEM micrographs (b) and cell size (c) of TPUGF samples as the function of graphene content.

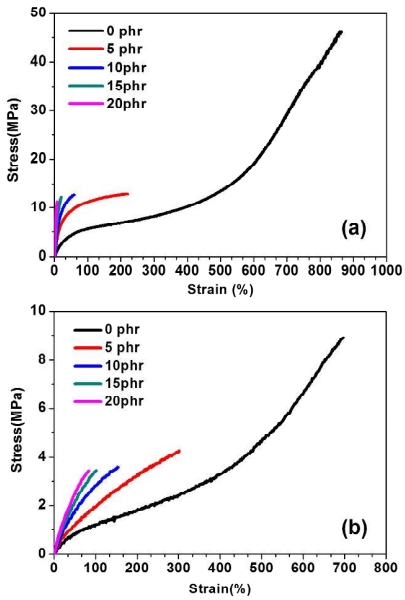

Fig. 3 Stress-strain curves of TPUG (a) and TPUGF (b) as the function of graphene content.

clear that TPUGF presents an uniform cell structure, and the increase in graphene content tends to decrease the cell size of TPUGF from 12.7 um for TPUGF0 to 7.6 um for TPUGF20 (Fig. 2c). This is probably due to the increased viscosity solution at high graphene loading, which restrains the cell growth process.[37]

3.2 Mechanical properties of TPUG and TPUGF

The representative stress–strain curves of TPUG and TPUGF under a tensile rate of 500 mm/min are presented in Fig. 3. TPUG0 exhibits a typical elastomer stress-strain curve, where an approximately linear region at low strain is followed by the plateau region. At strain higher than 600%, the stress increases due to strain hardening. TPUGF0 presents the similar stress–strain curve with that of TPUG0, characterized by soft and high ductility. The addition of graphene affects the stress-strain curve of TPU significantly, and the as-obtained TPUG with various graphene loading exhibits a brittle characteristic. In the case of TPUGF, it is still brittle, but its ductility increases obviously in relative to the unfoamed counterpart.

Table 2 lists the mechanical properties of TPUG and TPUGF. The increased Young's modulus (E) of TPUG and TPUGF with graphene loading is caused by the reinforcing effect of graphene.[31,38] However, the incorporation of graphene reduces significantly the elongation at break of TPU. The reason is due to the aggregation of graphene (Fig. S1) within TPU matrix, which may act as defects during the tensile testing process and decreases the elongation at break of TPUG.[20,38] With the introduction of cell structure, it is inspiring to find that the elongation at break of TPUGF samples is much higher than the corresponding TPUG samples.

3.3 Elasticity of TPUG and TPUGF

The elasticity of TPUG and TPUGF has been characterized by the hysteresis energy loss and residual strain in the cycle tensile test. The typical load-unload curves of TPUG0 and TPUG5 at an increasing strain level are presented in Fig. 4a and 4b. The hysteresis energy and residual strain at different strain level have also been calculated and fitted into smooth curves, as presented in Fig. 4c and 4d. TPUG5 and TPUG10 underwent the cycle test at the same condition until the samples were broken, TPUG15 and TPUG20 were too brittle to be performed

Table 2 Mechanical properties of TPUG and TPUGF as the function of graphene content

Graphene content (phr)	Young's modulus (MPa)		Tensile strength (MPa)		Elongation at break (%)	
	TPUG	TPUGF	TPUG	TPUGF	TPUG	TPUGF
0	15.2 ± 2.3	2.7 ± 0.3	46.3 ± 3.4	8.9 ± 1.0	863.3 ± 73.5	696.7 ± 20.4
5	41.7 ± 3.6	3.9 ± 0.2	12.9 ±1.2	4.5 ± 0.5	220.0 ± 16.2	301.7 ± 35.5
10	62.4 ± 5.8	5.0 ± 0.3	12.7 ± 0.3	3.6 ± 0.4	58.8 ± 5.6	155.0 ± 15.4
15	83.1 ± 2.4	6.8 ± 0.2	12.2 ± 0.6	3.5 ± 0.7	20.0 ± 5.7	101.7 ± 10.1
20	96.9 ± 2.7	7.8 ± 0.6	11.3 ± 0.8	3.3 ± 0.4	8.3 ± 6.2	83.3 ± 7.6

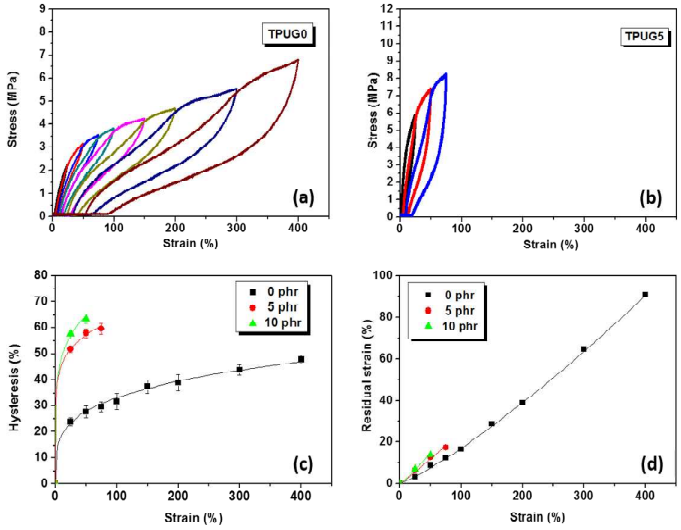

Fig. 4 Elasticity properties of TPUG samples. (a) Typical cycle tensile test of TPUG0 with a stepwise increase of strain; (b) Typical cycle tensile test of TPUG5 with a stepwise increase of strain; (c) Hysteresis energies of TPUG samples versus strain; (d) Residual strain of TPUG samples versus strain.

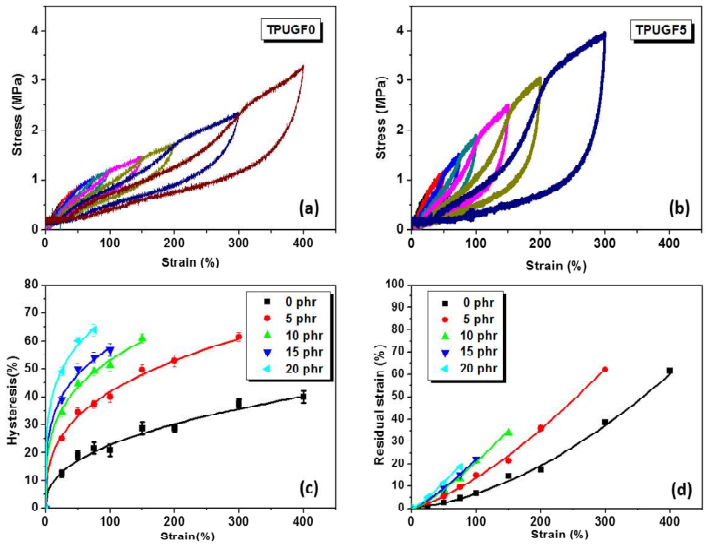

Fig. 5 Elasticity properties of TPUGF samples. (a) Typical cycle tensile test of TPUGF0 with a stepwise increase of strain; (b) Typical cycle tensile test of TPUGF5 with a stepwise increase of strain; (c) Hysteresis energies of TPUGF samples versus strain; (d) Remain strain of TPUGF samples versus strain.

the cycle test, so only the data of TPUG0, TPUG5, and TPUG10 were presented here. Firstly, it is obvious that the hysteresis of TPUG sample is strain dependence, which demonstrates that there is more hysteresis generated at higher strain. Subsequently, comparing to TPUG0, the hysteresis of TPUG increases greatly with increasing graphene content. The residual strain shows similar trend as the hysteresis curves: bigger strain, bigger residual strain; higher graphene content, bigger residual strain. However, the residual strain-strain curves are almost linear, while the curve of hysteresis versus strain tends to be stable at higher strain. This means that the residual strain of TPUG samples is much more sensitive to strain than that of hysteresis.

The typical load-unload curves of TPUGF0 and TPUGF5 at an increasing strain level were shown in Fig. 5a and 5b. The hysteresis and residual strain at different strain levels were calculated and the results were shown in Fig. 5c and 5d, respectively. Similar results could be concluded as it did in the case of TPUG. The hysteresis and residual strain are higher at larger strain or graphene content.

The elasticity of TPUG and TPUGF samples has been compared below. Taking the hysteresis data for example, the hysteresis of TPUGF0 is 39.8% at 400%, reduced by 18.0% comparing with TPUG0 (47.8%); The hysteresis of TPUGF5 is 44.7% at 75%, reduced by 14.9% comparing with TPUG5 (59.6%); For the sample containing 10 phr graphene, the reduction is 13.5% at 50% strain. From above results, it is observed that the TPUG show more hysteresis (more energy loss) than TPUGF samples at the same strain, and the difference of hysteresis between TPUG and TPUGF becomes larger as graphene content increases. Namely, the elasticity of TPUG increases with the introduction of porous structure.

To understand the influence of foam structure on the elastic behaviour of TPUG and TPUGF samples, further experiments were performed for samples without graphene below. We conducted cycle test with five times load-unload for typical TPUG0 and TPUGF0 at a fixed strain of 43%, using a constant tensile rate of 25 mm/min. In Fig. 6a and 6b, both TPUG0 and TPUGF0 show the significant Mullins effect (cyclic softening). The cycle softening, which shows a lower initial modulus in the second and subsequent load-unload cycle, can be explained by breakage and restructure of hard segments domains.[15] In Fig. 6c, the hysteresis of TPUGF0 is lower than TPUG0, which is in accordance with the results presented before. Moreover, the hysteresis decreases as the cycle number increases and then tends to steady at the fifth cycle. This phenomenon has been observed by other researchers and can be explained by destruction of the weak net-points and orientation of the molecular chains in a more favourable way, eventually an ideal orientated elastic network was formed after two cycles.[39, 40] From the results in Fig. 6 for samples without graphene, it is inferred that foam structure will have the same influence on the elastic behaviour of TPUG and TPUGF samples with graphene.

3.4 Conductivity of TPUG and TPUGF

Generally, the introduction of conductive fillers into insulating polymers will endow the resultant composites with good electrical conductivity.[41, 42] As shown in Fig. 7, the direct electrical conductivity for pristine TPU is marginally lower than 1.0×10^{-11} S/cm, while with the incorporation of only 5 phr graphene, this value increases dramatically to 1.5×10^{-3} S/cm. The increase is due to the formation of the conductive network in TPU matrix. Further increasing graphene loading to 20 phr will lead to a much higher conductivity of 1.3 S/cm.

In comparison with TPUG, the foamed counterparts, thus TPUGF, exhibit a much lower electrical conductivity. For example, the electrical conductivity of TPUGF20 is 1.4×10^{-5} S/cm, lower than the 1.3 S/cm of TPUG20. The possible reason is that the introduction of cell structure in to TPUG compromise the formation of the conductive network to some extent and decrease the paths for charge carriers moving.[18] Nonetheless, the level of the electrical conductivity of TPUGF is still sufficient for their some applications in semiconductors.[43]

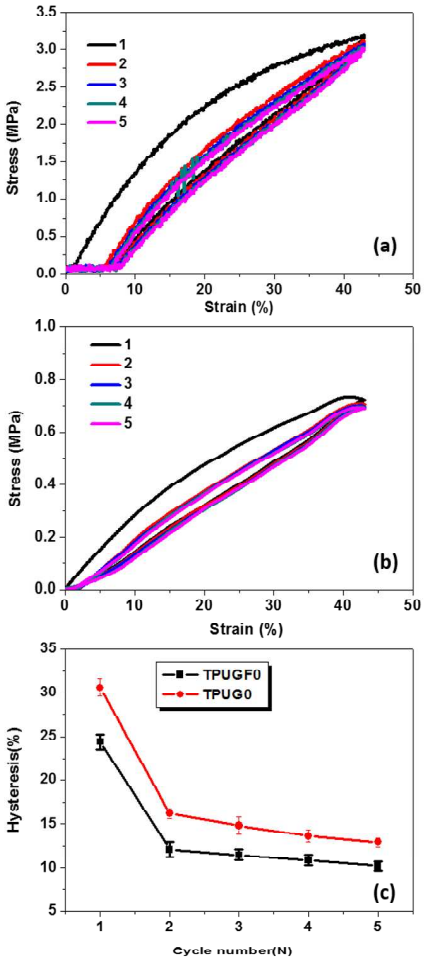

Fig. 6 Cycle tensile test of TPUG0 (a) and TPUGF0 (b) at a fixed strain of 43% with a tensile rate of 25 mm/min. The hysteresis of each cycle for TPUG0 and TPUGF (c) is obtained from the results in (a) and (b).

4 Discussion

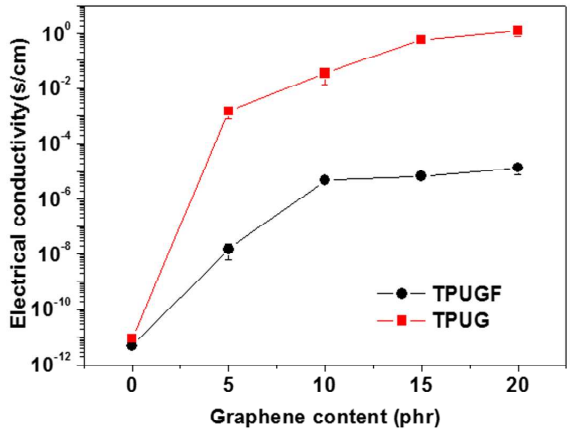

Fig. 7 Electrical conductivity of TPUG and TPUGF.

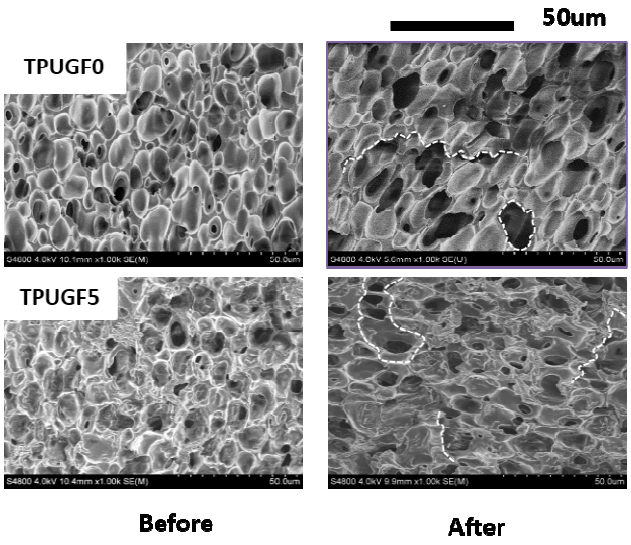

Fig. 8 SEM micrographs of TPUGF samples comparing the differences of cells before and after at least five cycle test. (The dash lines show typical cell coalescence and cell rupture).

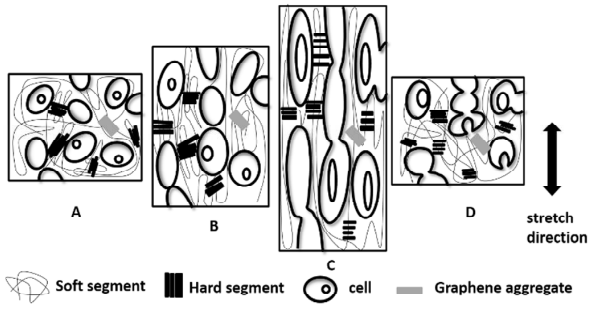

Fig. 9 Schematic picture to illustrate the deformation of cells and hard segments during extension and retraction in the first cycle: (A) before deformation, (B) during extension below the permanent set strain, (C) during extension at strain larger than the permanent set strain, and (D) during retraction to zero stress. The proportions between cell, cell wall, hard segment domain and graphene aggregate are not real. Not all the cells, hard segments and graphene aggregates are presented.

As the results presented above, the introduction of cell structure into TPUG composites has improved the strain at break and reduced the hysteresis. Consequently, the as-prepared TPUGF exhibits better mechanical and elasticity properties than TPUG does. It is rational to ascribe these to the cell structure within TPUGF, which is the biggest difference between them. Fig. 8 presents the cell morphology of TPUGF before and after at least five cycle tensile test, from which we can see clearly that the cells are elongated and preferentially orientated along the direction of deformation during the test. The elongation of cells can offset some deformation so that the real deformation of TPUGF is less than the TPUG counterpart. As a result, the disruption and the plasticity deformation of hard segment domains are restrained, leading to less the hysteresis loss for TPUGF.[44] Additionally, the local stress intensification is supposed to be the main reason the occurrence of cell coalescence that has been marked by dash lines in Fig. 8.

In Fig. 9, a schematic picture has been provided to illustrate the structure evolution of TPUGF during the cycle test process. The structure of TPUGF before tensile test has been sketched in Fig. 9A, in which open cells without deformation is located in TPUGF matrix.[45] When the sample is under low strain, the cells will be stretched along the extension direction and cell wall will become much thinner (Fig. 9B). Further increasing the strain over the permanent strain, some cells will reach to their limit, causing the occurrence of cell coalescence (Fig. 9C). In this process, some crystallites in the hard segment domains are destroyed partially and new crystallites are developed simultaneously.[46] After the release of the stress loaded on TPUGF (Fig. 9D), the cells can recovery almost to their original shape except for some cell coalescence as it has been observed in Fig. 8.

The addition of conductive fillers usually makes polymer composite brittle, high modulus, high hysteresis, and low repeatability. In the present work, however, Stretchable and flexible conductive TPUGF has been fabricated and the relationship between cell structure and elasticity were studied based on TPUGF with open cell structure. The main contribution of this study is that the introduction of bubble structure make material soft and can improve the stretching ability of material. The influence of different kind of cell structure like close cell or open cell with different porosity on the elasticity is needed in forthcoming work.

5 Conclusions

In summary, we have prepared stretchable conductive TPU/graphene nanocomposite foams through a facial WVIPS method. Compared with TPUG counterpart, the TPUGF samples have higher elongation at break and better elasticity because of the existence of microcellular structure. Firstly, the deformation of cells can offset partial deformation of the TPU matrix. Secondly, the cell walls can act as physical barrier for the destruction of hard segment and restrain further plastic deformation of hard segment domains under deformation. The lightweight, conductive, highly stretchable nanocomposite

foams present a new sight for applications in the field of novel electronics.

Acknowledgements

Financial support was provided by National High Technology Research and Development Program of China (863 Program, Grant No. 2013AA032003), National Natural Science Foundation of China (Grant No. 51473181 and 51573202) and China Postdoctoral Science Foundation (Grant No. 2015M570531).

Notes and references

1 T. Yamada, Y. Hayamizu, Y. Yamamoto, Y. Yomogida, A. Izadi-Najafabadi, D. N. Futaba and K. Hata, *Nat. Nanotechnol.*, 2011, **6**, 296-301.
2 T. Sekitani, Y. Noguchi, K. Hata, T. Fukushima, T. Aida and T. Someya, *Science*, 2008, **321**, 1468-1472.
3 Y. Hou, D. R. Wang, X. M. Zhang, H. Zhao, J. W. Zha and Z. M. Dang, *J. Mater. Chem. C*, 2013, **1**, 515-521.
4 H. B. Yao, J. Ge, C. F. Wang, X. Wang, W. Hu, Z. J. Zheng, Y. Ni and S. H. Yu, *Adv. Mater.*, 2013, **25**, 6692-6698.
5 R. Zhang, H. Deng, R. Valenca, J. H. Jin, Q. Fu, E. Bilotti and T. Peijs, *Compos. Sci. Technol.*, 2013, **74**, 1-5.
6 J. H. Kong, N. S. Jang, S. H. Kim and J. M. Kim, *Carbon*, 2014, **77**, 199-207.
7 C. Cochrane, V. Koncar, M. Lewandowski and C. Dufour, *Sensors*, 2007. **7**, 473-492.
8 I. Krupa and I. Chodak, *Eur. Polym. J.*, 2001, **37**, 2159-2168.
9 I. Novak, I. Krupa and I. Chodak, *Synthetic Met.*, 2002, **131**, 93-98.
10 M. Kubo, X. F. Li, C. Kim, M. Hashimoto, B. J. Wiley, D. Ham and G. M. Whitesides, *Adv. Mater.*, 2010, **22**, 2749-2752.
11 A. C. Siegel, D. A. Bruzewicz, D. B. Weibel and G. M. Whitesides, *Adv. Mater.*, 2007, **19**, 727-733.
12 M. Park, Y. Xia and U. Jeong, *Angewandte Chemie*, 2011, **50**, 10977-10980.
13 F. Xu and Y. Zhu, *Adv. Mater.*, 2012, **24**, 5117-5122.
14 M. Park, J. Park and U. Jeong, *Nano Today*, 2014, **9**, 244-260.
15 C. P. Buckley, C. Prisacariu and C. Martin, *Polymer*, 2010, **51**, 3213-3224.
16 Z. X. Chen and H. B. Lu, *J. Mater. Chem.*, 2012, **22**, 12479-12490.
17 U. Khan, P. May, A. O'Neill, J. J. Vilatela, A. H. Windle and J. N. Coleman, *Small*, 2011, **7**, 1579-1586.
18 E. Bilotti, R. Zhang, H. Deng, M. Baxendale and T. Peijs, *J. Mater. Chem.*, 2010, **20**, 9449-9455.
19 L. Lin, S. Liu, Q. Zhang, X. Y. Li, M. Z. Ji, H. Deng and Q. Fu, *ACS Appl. Mater. Interfaces*, 2013, **5**, 5815-5824.
20 J. T. Choi, D. H. Kim, K. S. Ryu, H. I. Lee, H. M. Jeong, C. M. Shin, J. H. Kim and B. K. Kim, *Macromol. Res.*, 2011, **19**, 809-814.
21 V. Dolomanova, J. C. M. Rauhe, L. R. Jensen, R. Pyrz and A. B. Timmons, *J. Cell. Plast.*, 2011, **47**, 81-93.
22 R. Rizvi and H. Naguib, *J. Mater. Res.*, 2013, **28**, 2415-2425.
23 J. D. Fromstein and K. A. Woodhouse, *J. Biomat. Sci. Polym. E.*, 2002, **13**, 391-406.
24 M. T. Khorasani and S. Shorgashti, *J. biomed. Mater. Res. B.*, 2006, **76B**, 41-48.
25 J. J. Guan, K. L. Fujimoto, M. S. Sacks and W. R. Wagner, *Biomaterials*, 2005, **26**, 3961-3971.
26 Y. Li, X. L. Pei, B. Shen, W. T. Zhai, L. H. Zhang and W. G. Zheng, *RSC Adv.*, 2015, **5**, 24342-24351.
27 B. Shen, W. T. Zhai, M. M. Tao, J. Q. Ling and W. G. Zheng, *ACS Appl. Mater. Interfaces*, 2013, **5**, 11383-11391.
28 W. T. Zhai, Y. J. Chen, J. Q. Ling, B. Y. Wen and Y. W. Kim, *J. Cell. Plast.*, 201y4, **50**, 537-550.
29 J. Q. Ling, W. T. Zhai, W. W. Feng, B. Shen, J. F. Zhang and W. G. Zheng, *ACS Appl. Mater. Inter.*, 2013, **5**, 2677-2684.
30 C. Lee, X. D. Wei, J. W. Kysar and J. Hone, *Science*, 2008, **321**, 385-388.
31 S. Stankovich, D. A. Dikin, G. H. B. Dommett, K. M. Kohlhaas, E. J. Zimney, E. A. Stach, R. D. Piner, S. T. Nguyen and R. S. Ruoff, *Nature*, 2006, **442**, 282-286.
32 M. Moussa, M. F. El-Kady, H. Wang, A. Michimore, Q. Q. Zhou, J. Xu, P. Majeswki and J. Ma, *Nanotechnology*, 2015, **26**, 075702.
33 K. L. Xu, G. M. Chen and D. Qiu, *J. Mater. Chem. A*, 2013, **1**, 12395-12399.
34 H. B. Zhang, Q. Yan, W. G. Zheng, Z. X. He and Z. Z. Yu, *ACS Appl. Mater. Interfaces*, 2011, **3**, 918-924.
35 F. Yavari, M. A. Rafiee, J. Rafiee, Z. Z. Yu and N. Koratkar, *ACS Appl. Mater. Interfaces*, 2010, **2**, 2738-2743.
36 J. A. Miller, S. B. Lin, K. K. S. Hwang, K. S. Wu, P. E. Gibson and S. L. Cooper, *Macromolecules*, 1985, **18**, 32-44.
37 H. C. Park, Y. P. Kim, H. Y. Kim and Y. S. Kang, *J. Membrane Sci.*, 1999, **156**, 169-178.
38 U. Khan, P. May, A. O'Neill and J. N. Coleman, *Carbon*, 2010, **48**, 4035-4041.
39 C. R. Desper, N. S. Schneider, J. P. Jasinski and J. S. Lin, *Macromolecules*, 1985, **18**, 2755-2761.
40 P. Ping, W. S. Wang, X. S. Chen and X. B. Jing, *J. Polym. Sci. Pol. Phys.*, 2007, **45**, 557-570.
41 A. Ameli, M. Nofar, S, Wang and C. B. Park, *ACS Appl. Mater. Interfaces*, 2014, **6**, 11091-11100.
42 A. Ameli, P. U. Jung and C. B. Park, *Carbon*, 2013, **60**, 379-391.
43 O. T. Ikkala, J. Laakso and K. Vakiparta, *Synthenic Metals*, 1995, **69**, 97-100.
44 R. M. Versteegen, R. Kleppinger and R. P. Sijbesma, *Macromolecules*, 2006, **39**, 772-783.
45 Q. Ye, Y. L. Xiang, F. X. Chen, W. L. Xu and H. J. Yang, *Mater. Lett.*, 2013, **100**, 23-25.
46 S. Toki, I. Sics, C. Burger, D. F. Fang, L. Z. Liu, B. S. Hsiao, S. Datta and A. H. Tsou, *Macromolecules*, 2006, **39**, 3588-3597.